Results in Engineering 21 (2024) 101730

Contents lists available at ScienceDirect

Results in Engineering

journal homepage: www.sciencedirect.com/journal/results-in-engineering

Impact response of filament-wound structure with polymeric liner: Experimental and numerical investigation (Part-A)

Mohammad Azeem [a,*], Hamdan H. Ya [a,**], Mohammad Azad Alam [i], Masdi Muhammad [a], Salit M Sapuan [b,c], Mukesh Kumar [d], Lokman Gemi [e], Ammar Maziz [f], Ahmad Rasdan Ismail [g], Sanan H. Khan [h,***]

[a] Mechanical Engineering Department, Universiti Teknologi PETRONAS, Seri Iskandar, 32610, Malaysia
[b] Laboratory of Biocomposite Technology, Institute of Tropical Forestry and Forest Products, Universiti Putra Malaysia, 43400, UPM Serdang, Malaysia
[c] Department of Mechanical and Manufacturing Engineering, Universiti Putra Malaysia, 43400, UPM Serdang, Malaysia
[d] Department of Mechanical Engineering, Indian Institute of Technology, Ropar, Punjab,140001, India
[e] Meram Vocational School, Necmettin Erbakan University, 42000, Konya, Turkey
[f] ENSTA Bretagne, FRE CNRS 3744, IRDL, F-29200 Brest, France
[g] Department of Environmental Health Sciences, College of Health Sciences, University of Sharjah, 27272, Sharjah, United Arab Emirates
[h] Department of Mechanical and Aerospace Engineering, United Arab Emirates University (UAEU), Al Ain 15551, United Arab Emirates
[i] Interdisciplinary Research Centre for Renewable Energy and Power System (IRC-REPS), Research Institute, King Fahd University of Petroleum and Minerals (KFUPM), Dhahran 31261, Saudi Arabia

ARTICLE INFO

Keywords:
Composite pipelines and pressure vessels
Filament winding
Polymer composite
Low-velocity impact
Polymeric liner
Damage

ABSTRACT

Filament wound pipelines and Type IV composite pressure vessels (CPVs) constitute polymeric liners and are extensively used to transport and store petroleum products, hydrogen, and compressed natural gas (CNG). The polymeric liner does not share much pressure load; hence, the composite layers share most of the load. The situation gets worse under transverse impact loads on such structures. For the polymeric liner to be effectively used in pipelines and CPVs, it is crucial to study impact response through testing and computational methods. This article presents experimental and numerical investigations of the transverse low-velocity impact response of filament wound samples. High-density polyethylene (HDPE) liner was adopted, and carbon fiber (T700) continuous filaments with epoxy resin were wound over the liner with several layers. A drop-weight impact loading with 40 J energy has been applied to the fabricated samples. The development of impact damage was assessed using the finite element method, and the damage modes have been discussed. The specimen remains unperforated at the chosen energy level. Though HDPE is ductile, however at impact loads liner damage was encountered, displaying a brittle fracture. At higher strain rates, the material reaches its brittle fracture point sooner, leading to failure. The material breaks as brittle due to its inability to dissipate impact energy quickly, resulting in fracturing instead of deformation. Fiber damage was scarcely seen; however, matrix damage has been the dominant failure mode at the chosen impact energy. Comparisons between the simulation and test findings were made, and they agreed on force-time and force-displacement histories.

1. Introduction

Fiber-reinforced composite pipes are gaining popularity in various industries due to their high specific stiffness, strength, corrosion resistance, and thermal insulation, and their application in cylindrical composite structures is gaining interest due to advancements in manufacturing technology [1]. The evolution of gas storage pressure vessels has been driven by the need to improve safety, reduce weight and

* Corresponding author.
** Corresponding author.
*** Corresponding author.
E-mail addresses: mazeem.me@zhcet.ac.in (M. Azeem), hamdan.ya@utp.edu.my (H.H. Ya), mohammad.alam@kfupm.edu.sa (M.A. Alam), masdimuhammad@utp.edu.my (M. Muhammad), sapuan@upm.edu.my (S. M Sapuan), mukesh.kumar@iitrpr.ac.in (M. Kumar), lgemi@erbakan.edu.tr (L. Gemi), ammar.maziz@ensta-bretagne.org (A. Maziz), a.binismail@sharjah.ac.ae (A.R. Ismail), shkhan@uaeu.ac.ae (S.H. Khan).

https://doi.org/10.1016/j.rineng.2023.101730
Received 14 October 2023; Received in revised form 10 December 2023; Accepted 29 December 2023
Available online 30 December 2023

cost, and increase efficiency and performance. Composite pressure vessels, Types III and IV, are used in CNG vehicles for lightweight, strong mechanical characteristics [2]. Early fuel gas storage pressure vessels were made of steel, but they were heavy and prone to corrosion. In recent years, composite materials like fiber-reinforced plastic (FRP) have gained popularity due to their lightweight, corrosion-resistant properties. FRP vessels consist of layered sheets of reinforcing fibers (carbon, Kevlar, or glass fibers) embedded in a resin matrix [3,4].

Pressure vessels are categorized into five types: full metallic tanks (Type I), composite hoop-wrapped tanks with metallic liners (Type II), fully composite overwrapped tanks with metallic liners (Type III), fully composite overwrapped tanks with polymeric liners (Type IV), and composite linerless tanks (Type V). These are commonly used for fuel storage in cars, especially natural gas and hydrogen-powered ones, due to their superior strength-to-weight ratio, corrosion resistance, and fatigue strength [4–6]. Type IV vessels are ideal for fuel gas storage due to their low energy density and high-pressure ranges. They are particularly suitable for small, transportable applications like fuel tanks in automobiles or gas transport trailers due to their low weight and excellent mechanical strength [7]. CPVs offer weight savings as compared to Type I metallic pressure vessels but require specific mechanical design, fabrication, and testing requirements. They require detailed analysis due to composite layers and inner liner interaction, and fail criteria are diversified compared to metallic pressure vessels [8,9].

Filament winding is a cost-effective, reliable fabrication technique for composite structures, pipes, transmission pipelines, pressure vessels, and driveshafts, producing strong, lightweight, and quality-regulated structures in various industries [10–12]. The FRP pipes made through this process are utilized for a range of applications, including the transportation of oil and storage of natural gas, chemical, and industrial liquids under pressure [13,14]. Various studies examined filament wound structures and their parameters. The crush response of filament wound tubes with metallic liner was studied in Ref. [15], where the filament winding technique demonstrated the most significant enhancement in crashworthiness of CFRP/Al hybrid tubes, outperforming vacuum bag forming and nested manufacturing processes. Dry filament wound composite tube buckling due to external pressure was studied in Ref. [16] through experimental and numerical methods. The study found that tubes with a diameter-to-thickness ratio below 20:1 fail by buckling, while those with a higher ratio experience failure primarily due to in-plane shear and delaminations.

Another experimental study [17] evaluates the pre- and post-impact behavior of filament-wound hybrid pipes. The study found that specimens with alternative fibers showed better impact resistance under the same impact energy conditions. Carbon fiber-reinforced epoxy specimens had the worst impact damage tolerance despite having the highest compressive strength before impact and the highest reduction of 62% in residual compressive force after impact. The effect of thickness and stacking of thermoplastic composite pipes (TCPs) against burst pressure was studied in Ref. [18]. The analysis and FEA methods confirmed that the burst pressure of a TCP increases as the number of reinforcement plies increases, and the optimal winding angle associated with maximum burst pressure varies with the thickness of the laminate layer. Axial quasi-static compression was done in a study on filament-wound CFRP hybrid tubes with aluminium liner [19]. The study found that winding angle and wall thickness significantly impact failure modes and crushing characteristics of CFRP and hybrid tubes. Increased winding angle decreased specific energy absorption, energy absorption, and peak crushing force, while increased tube thickness enhanced these properties.

Composite pipelines and cylinders can be damaged by external forces like foreign objects or vibrations. Low-velocity impacts can cause various damage types, viz., fiber breakage, matrix cracking, and fiber-matrix debonding. Barely visible impact damage (BVID) is generally caused by these low-velocity impacts, causing small cracks and indentations that are difficult to detect without inspection [20,21]. BVID can weaken composites, increasing their failure risk, often invisible until it's already weakened. Impact tests on flat composite laminates assessed this issue [22–27]. Various fibers (glass and basalt fiber) with different matrices were tested against low-velocity impact in Ref. [24] to study the stacking effect and thickness dependence. The stacking sequence of glass fiber specimens did not affect penetration energy, but quasi-isotropic specimens showed lower indentation under the same impact energy, and basalt laminates showed lower indentation depths. A study investigates the impact response of carbon/glass hybrid filament wound composite pipes under different energy levels. Results reveal damage formation, with CGG stacking showing higher impact resistance and GCG stacking showing better damage formation response [28]. Another study compares the low-velocity impact performance of basalt fabric epoxy prepreg and aluminium sheets in fiber metal laminates, finding them competitive with monolithic plates [27]. Basalt fiber metal laminates show significant impactor size influence and positive response, competing with monolithic aluminium plates, despite concerns about the aluminium/basalt interface.

Some research has been done to assess the low-velocity impact performance of filament wound tubular or cylindrical structures. The experimental study [29] studied the effect of stack sequence in filament wound pipes with carbon-glass/epoxy layers with a thin polymeric liner. The study found that the stacking sequence of layers significantly impacts impact resistance behavior, with the fiber content ratio also playing a role. Positioning basalt fiber on the impacted side improves energy absorption and impact resistance. The transverse low-velocity impact was conducted in Ref. [30], and the influence of the stacking sequence was determined. Impact tests on cylinders reveal that the stacking sequence is a crucial parameter for cylinder impact behavior.

An experimental and statistical study was conducted on $(\pm 55^{\circ})_3$ E-glass/epoxy filament wound pipes, and several damage modes were encountered [31]. The study found no significant difference in force values with increased impact velocity, but force values increased. Higher rebound energy values were obtained with increasing impact velocity. Absorbed energy values were found dependent on impact velocity, while rebound energy values were independent. The Weibull analysis results indicated that higher impact velocity resulted in more reliable results.

The influence of impact loading on the fatigue performance of hybrid pipes with internal pre-stress has been studied [32]. The study reveals that as pre-stress loading increases before impact loading, impact damage decreases, and fatigue life enhances. The maximum vertical displacements decrease with increasing pressure load, indicating damage formation. High internal pre-stress values increase resistance to bending, and increased pre-stress levels increase fatigue damage area. A computational model including damage was created in a study to forecast the failure of carbon fiber-based filament-wrapped composite tubes against radial compressive loads [33]. The study evaluates three stacking sequences, revealing that hoop layers and $\pm 75^{\circ}$ non-geodesic layers provide maximum compressive load to the composite tube due to reinforcement wound closer to the loading direction. The failure modes are predominantly delaminations, confirmed through numerical and experimental analyses.

Another study [34] investigated the burst behavior of polymeric liners. Experimental hydrostatic tests were conducted on reduced scale and actual liner models, focusing on the design and failure prediction of composite laminate shell and polymeric liner using Tsai-Wu and Von Mises criteria, using Finite Element Analysis (FEA). The post-impact axial compression response of filament-wound samples was studied in Ref. [35]. The study reveals that pipe diameter increases in low velocity impact loading, reducing radial buckling load and altering penetration-dominant damage to bending and delamination-dominant damage type. This effect is more pronounced when exposed to compression after impact (CAI) loading, suggesting that impact pre-damage affects compressive strength and damage development.

High impact loading rates can alter fiber-reinforced polymer

composites' mechanical properties, including elastic modulus and strength, before strain softening and failure. Factors like failure mechanisms and fracture energy must be considered to ensure performance and structural integrity in impact or dynamic loading conditions [36]. Type IV vessels face increased safety concerns due to their polymeric liner and internal/external loading. There are no recognized standards for CPVs or tubes under transverse impact loadings, necessitating certification by organizations and pressure vessel standards [37]. Consequently, Investigating impact behavior and damage mechanisms in vessel structures can aid in safer product development [38].

1.1. Polymeric liners

Pipelines are essential for transporting crude oil and natural gas, but they are susceptible to internal corrosion due to corrosive contaminants like CO_2, H_2S, water, and microbes. The most common forms of corrosion are CO_2 and H_2S corrosion. Factors such as temperature, corrosive gases, water chemistry, flow velocity, and pipe material surface condition also contribute to corrosion. Measures to mitigate this include selecting appropriate materials, corrosion inhibitors, metallic and non-metallic linings, and coatings. Non-metallic pipe materials like polymers are used as internal liners, while thermoplastic liners can be used for pipe rehabilitation [39,40]. Polymeric liners gain popularity in Type IV CPVs due to their lightweight, cost-efficient, corrosion-resistant, fatigue life, and hydrogen embrittlement avoidance [41–43]. Rotational molding offers low manufacturing and tooling costs and produces flexible, impact-tolerant polymeric liners [44]. Polyethylene and polyurethane are common liners in Type IV pressure vessels due to their flexibility and resistance to chemicals. Low-density polyethylene (LDPE), polyamide, and polypropylene are also used. When choosing a liner material, factors like gas permeation, operating temperature, pressure, and desired corrosion resistance must be considered [45–47].

HDPE is a lightweight, strong, and environment-resistant semi-crystalline thermoplastic polymer used in construction materials, pressure vessel liners, industrial pipelines, and plastic bottles [48,49]. HDPE is a low permeability, chemical and UV-resistant material suitable for pressure vessels. It is non-toxic, heat-resistant up to 120 °C, and offers strength and flexibility for Type IV vessel liners. Its ductility at low strain rates makes it a cost-effective choice. However, a material that is ductile at low strain rates may become brittle at high strain rates [50]. Many studies have utilized HDPE liners in pressure vessels [51–54], and a few have used a blend of LLDPE/HDPE [8,55].

1.2. Effects of impact loading

Composites use fibers or reinforcing elements oriented in specific directions for maximum strength and stiffness. However, along the thickness direction, mechanical properties may be reduced due to inadequate support in the through-thickness direction [56,57]. Type III and Type IV CPVs differ in construction, materials, and load sharing between the liner and composite layers. In Type III, metallic liners share a significant pressure load with composite layers, while Type IV CPVs have polymeric liners sharing lesser part of the load. Low-velocity impacts, such as unintentional drops, heavy tools, falling cylinders, or road crashes, can cause damage, leading to early failure and difficulty in detection [58–60]. Low-velocity impact can cause delamination and fiber breakage in composite laminates without visible damage, causing structural degradation and potentially lowering efficiency. Internal damage is often unseen and invisible [61–63]. On the other hand, the impact phenomenon and the damage it causes are complex due to varying effects and parameters. The significant difficulties are the nonlinear dynamic reactions, i.e., the contact between impactor and sample (target) and large displacements, load-bearing layers, layer thickness, variable composite properties, and the simultaneous occurrence of varying damage mechanisms [64,65].

The experimental and numerical research aims to assess the low-velocity impact response of carbon-fiber wrapped structures with polymeric liners. It addresses a gap in knowledge about composite overwrapped structures' behavior under low-velocity impacts, particularly in filament wound structures. The research on polymeric liners' response to low-velocity impact is significant due to the lack of existing studies. The experimental phase involves sample fabrication and testing using a low-velocity impact instrumented machine, demonstrating a commitment to rigorous testing methodologies for precise and quantifiable data.

This study assessed the low-velocity impact response of carbon-fiber-wrapped structures consisting of polymeric liners and was studied experimentally and numerically. The composite overwrapped sample behavior was understood with polymeric liners' response, which has scarcely been studied against low-velocity impact in the context of filament wound structures. The fabricated samples were experimentally tested using a low-velocity impact instrumented machine. The experimental tests were simulated utilizing the finite element tool. The fiber and matrix failure modes against impact loading were discussed in this part (the delamination failure mode will be presented in Part-B). The Hashin strength-based criterion was employed to predict the onset and progression of failure in composite materials. It is based on the concept of the strength of the material in different directions, and it defines the contours of failure in a composite material.

2. Materials and methods

The samples were produced through filament winding using a plastic liner as a mandrel, reflecting Type IV CPV construction. The research methodology involves four phases. In the first phase, the fabrication of samples was executed after selecting materials through the wet filament winding technique [66], followed by experimental activity and numerical analysis in the second and third phases. Then, after the comparison and results, discussions were held in phase IV. The research flow adopted is shown in the flowchart of Fig. 1.

2.1. Materials

Fiber filaments wound continuously on a mandrel are used in filament-wound pipes and CPVs to create composite specimens. T700 carbon fiber is popular for aerospace, automotive, and sports goods due to its strength, stiffness, and low weight. It is lightweight, easy to use, and resistant to corrosion. Epoxy resins, which bond well with fibers, offer strength, durability, and excellent chemical and fatigue strength. These materials are used in various applications due to their excellent chemical and fatigue strength [67,68]. Epoxy resins offer superior properties and resistance to moisture, corrosive liquids, and environments, offering a favorable cost-to-performance ratio compared to polyester or vinyl ester resins [69]. T700 carbon fiber and epoxy are commonly used in composite materials for aerospace, automotive, and sporting goods applications owing to their high strength, stiffness, and flexibility, minimizing cracking risks [70]. Toray™ Industries, Inc., Japan, provided the fiber for this study.

2.2. Fabrication method of filament wound structure

Fig. 2 (a) illustrates how filament-wound composite tubular structures were created utilizing a filament winding machine at SIRIM Sdn. Bhd. (Malaysia). Carbon/epoxy layers were wound over an HDPE mandrel to create filament wound pipes. Multi-angle winding comprising hoop, helical, and polar winding patterns are adopted. The first and the last layers are hoop winding; the polar and helical winding are wound between them. The winding angles and other details adopted in this study are given in Table 1. Carbon fiber tows are run through an epoxy resin bath. The roller encounters the fibers as it rotates, coating them with resin. Resin-coated carbon fiber tows were then wrapped

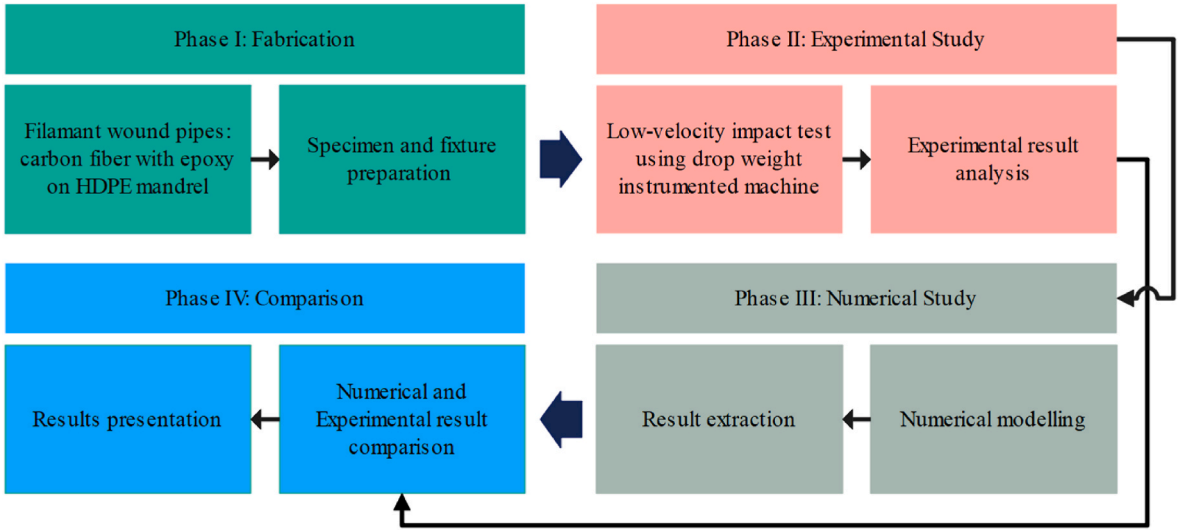

Fig. 1. Research methodology flowchart. Phase I involves preparatory work comprising the fabrication of specimen and sample fixture. In Phase II, experimental studies were undertaken, which was followed by numerical modeling in Phase III. Finally, a comparison and combined result analysis was done in Phase IV.

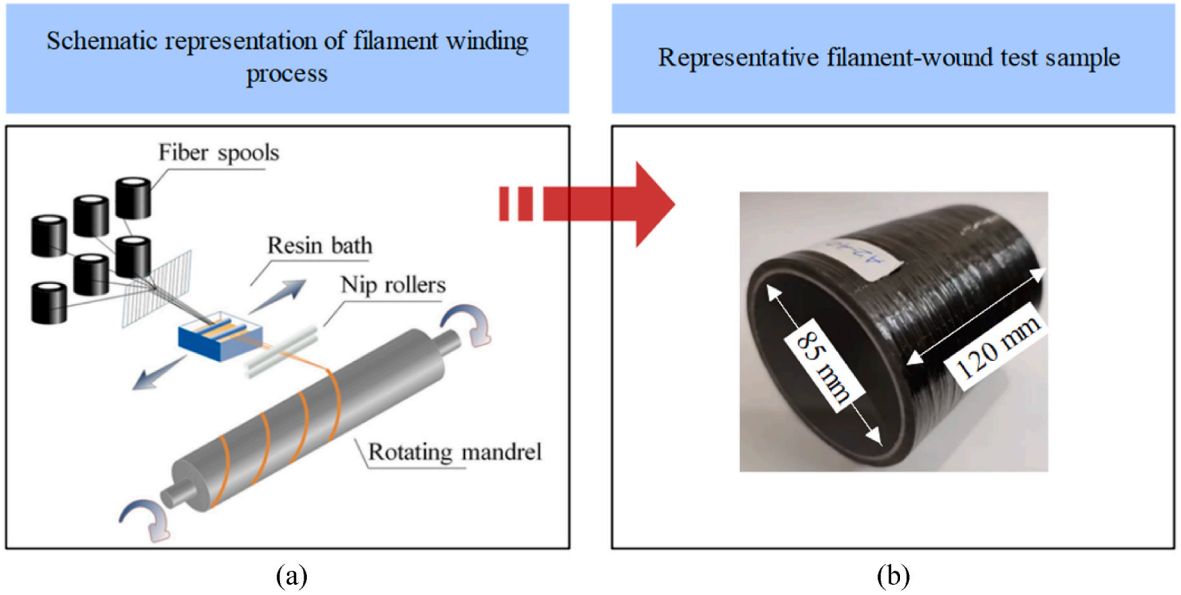

Fig. 2. Schematic representation of (a) wet filament winding procedure [71] showing the mandrel and fiber winding on it and (b) fabricated representative sample.

Table 1
Mechanical properties of composite plies. Various elastic parameters for the composite layers of Carbon/epoxy are given, and the same is used in FE analysis (symbols have their usual meaning).

Description	Details
Composite properties	
Density	$\rho = 1420$ kg/m^3
Elastic properties	$E_{11} = 98.34$ GPa, $E_{22} = 6.45$ GPa, $E_{33} = 6.45$ GPa, $\upsilon_{12} = 0.30$, $\upsilon_{23} = 0.11$, $\upsilon_{13} = 0.30$, $G_{12} = 2.69$ GPa, $G_{23} = 2.89$ GPa, $G_{13} = 2.69$ GPa
Strengths	$X_{11t} = 2058$ MPa, $X_{11c} = 1029$ MPa, $X_{22t} = 24.3$ MPa, $X_{22c} = 34.4$ MPa, $S_{12} = 18.3$ MPa
Winding parameters	
Winding angles	$[90/+8/-8/+15/-15/+30/-30/+55/-55/90]^o$
Average ply thickness	0.45 mm
Fiber type	Carbon fiber (T700)
Resin	Epoxy
Lining material	HDPE (PE100)

around the rotating pipe mandrel. The fiber orientation was adjusted using a horizontal carriage motion, and epoxy-coated fibers were coiled/wound around a pipe mandrel. The dispensing fiber is then cut when the sample is complete. The sample was then placed in an oven to cure. Curing is a crucial step in manufacturing composites, ensuring strength and durability. The curing process lasted 24 hours at 60 °C. The cured composite pipes were then cut into specific size samples for testing. The inside diameter of the HDPE pipe is 85 mm, and the wall thickness is 1.5 mm. The illustration of the representative sample is shown in Fig. 2 (b). The samples had an average thickness of 6 mm, including HDPE lining.

2.3. Material model

Filament-wound composites are materials made by winding fibers around a mandrel, as in cylindrical structures. Modeling these composites is crucial for predicting their mechanical behavior, focusing on high-modulus fibers and polymer matrix properties. The elastic properties of fibers, typically carbon or glass fibers, and the properties of the

matrix material, typically polymer resin, must be determined to account for the anisotropic behavior of filament-wound composites. Orientation-dependent properties are crucial in composite behavior, and methods like micromechanics and homogenization techniques are used to relate it to constituent properties.

Unidirectional composite materials are often represented as orthotropic laminas, with fibers aligned along a direction. The orientation of fibers, expressed in winding angles (θ), is a critical parameter that significantly influences the anisotropic behavior of the lamina, affecting the mechanical properties of these materials and stress levels in pressure vessels [72]. Orthotropic properties of each lamina, with their orientation, can be defined for the whole stack. Key elastic constants like Young's moduli, Poisson's ratios, and shear moduli are needed to describe the lamina's response to different loading conditions along and perpendicular to the fiber direction. Failure analysis in unidirectional composites uses specific criteria to account for fiber-dominated and matrix-dominated failure modes, such as fiber breakage and matrix cracking, defined through the Hashin criterion, etc. Micromechanical models like the Rule of Mixtures, Chamis's equations and Halpin-Tsai rule estimate lamina's effective elastic properties based on fibers and matrix properties. An accurate material model for filament-wound composites requires understanding of individual components, orientation-dependent properties, failure criteria, numerical simulations, and rigorous experimental validation, ensuring it accurately reflects the complex mechanical behavior in practical applications. The liner's mechanical properties and those of the carbon fiber-epoxy are shown in Table 1. The properties are found using the Chamis model [73]. Table 2 provides the details of the liner material. The damage model is discussed in section 3.5.

2.4. Investigation programme

Impact testing of composites employing a drop tower, a striking mass, and a clamping apparatus to hold the sample is specified in detail in the ASTM D7136 standard. The equipment is equipped with various gauges and sensors to gather relevant information. Although the test technique is primarily intended for evaluating the damage resistance of laminated plates, a specialized fixture can be used for cylindrical specimens, as demonstrated in this study. The details of impact testing and numerical study are given in Table 3.

2.4.1. Impact testing

The IMATEK drop-weight apparatus was used to evaluate composite samples during an impact event, Fig. 3. The potential energy of the drop weight was determined based on the mass and falling height of the impactor. Data acquisition (DAQ) capabilities were utilized to control the drop weight, configuring test settings, and collecting data.

The system stores information about impact force and energy absorption. A V-block clamping fixture was used to secure the sample during the test. A 16 mm diameter hemispherical nosed impactor was employed, as they resemble natural impact objects, making them more relevant for impacting samples. The impact tests involved an impactor with a weight of 5.101 kg and an energy level of 40 J. The apparatus had an anti-rebounding mechanism to prevent the impactor from hitting the specimen again. A force transducer measured contact force, and a linear variable differential transformer tracked displacement readings. Average results were presented based on three identical specimens.

Table 2
The mechanical properties of the liner [74].

Liner properties	Details
Material	HDPE (PE100)
Density, kg/m^3	958
Tensile modulus, MPa	900
Yield stress, MPa	23

Table 3
Details of experimental impact testing and numerical study.

Parameter	Experimental impact testing	Numerical impact simulation
Apparatus	Drop weight impact equipment	Platform: Abaqus/explicit
Energy level	40 J	The experimental velocity with impact energy equivalent to 40 J
Impactor	Hemispherical, 16 mm	Short impactor nose
Impactor material	Steel	Rigid instance (non-deformable)
Mass	5.101 kg	Inertia assigned to reference point
Composite layer material	Fiber: Carbon fiber (T700) Resin: Epoxy	Deformable, orthotropic SC8R continuum shell elements
Liner	HDPE (P100)	Deformable, isotropic SC8R continuum shell elements
Fixture details	V-block fixture with mountings	Rigid V-block

Force-displacement, force-time, and energy-time histories were obtained to analyze impact damage and energy-absorbing capacities. The impactor was lifted through a chain-pulley arrangement, and the sample was removed and visually examined.

3. Finite element analysis

The study developed a finite element (FE) model using the Abaqus solver to support low-velocity impact testing outcomes. The model accurately represents the sample and testing environment. Abaqus includes built-in failure criteria for composites, such as Hashin's criteria [75]. Abaqus can predict damage onset in composites using Hashin's criterion and the damage evolution law.

3.1. Composite specimen geometry

The study used the layer-by-layer technique for FE modeling of composite samples [76], representing pressure vessels as stacks of layers with different plies of material. Continuum shell elements are ideal for modeling thin-walled structures like pressure vessels. Specifying accurate material properties, orientation, and lay-up, along with specific boundary and loading conditions to reflect real-test scenarios, they can handle anisotropic material behavior, making them suitable for fiber-reinforced composites. SC8R continuum shell element accurately represents structures' response to large deformations and high strain rates during impact events. These elements can also capture nonlinear behavior, such as plasticity and creep, essential for accurately representing structures under extreme loads. Advanced material models, such as damage and failure models, can be applied to SC8R elements to predict damage and failure onset and progression during impact events. Previous studies have successfully utilized SC8R elements for modeling composite pipes, shells, and pressure vessels [77–80]. Continuum shell elements with reduced integration technique ensure high accuracy and stability and minimize computational cost, with eight nodal points for superior accuracy compared to fewer nodal points. The study used an orthotropic material model for the composite sample, with each ply represented by a smooth mesh, including a single element running in the thickness direction. The plies were deformable bodies, and winding angles were defined for each ply. Fig. 4 (a) illustrates the meshed sample, while Fig. 4 (b) and 4 (c) provide details on meshing and element types. The winding angles are defined for each ply, as shown in Fig. 5 (a).

3.2. Impactor modeling

The impactor can be modeled in several ways: as a rigid body with no assigned properties, real rigidity with allocated properties through the

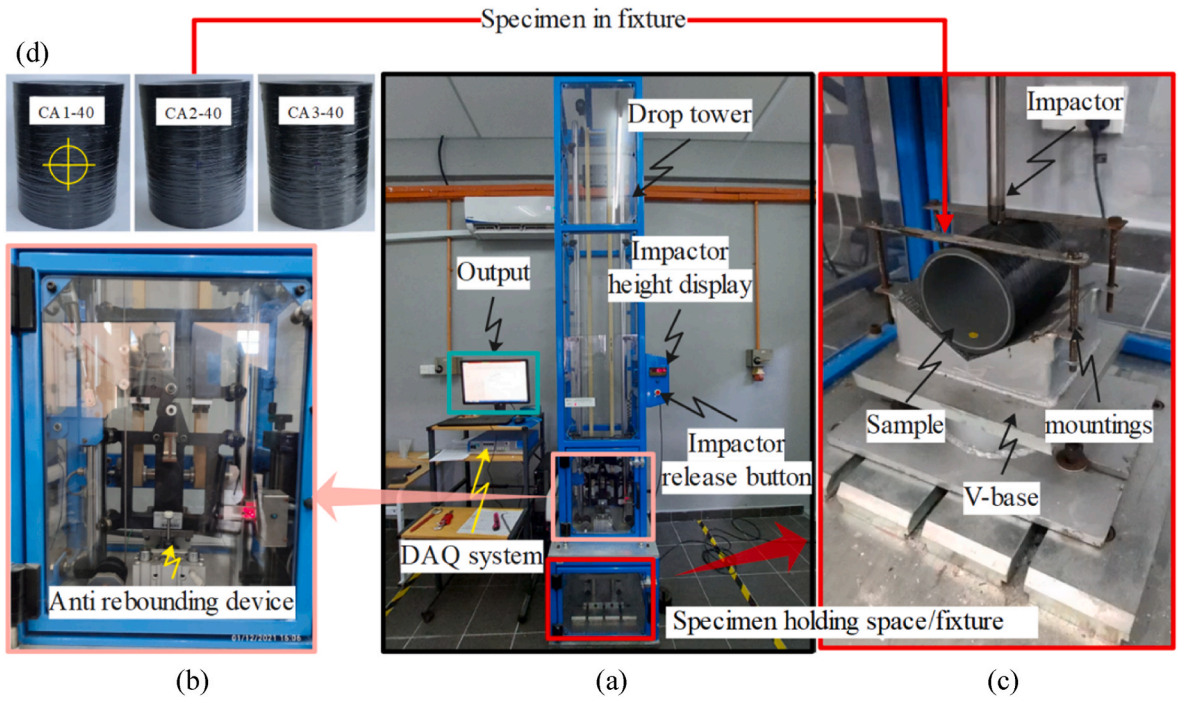

Fig. 3. Experimental set-up: (a) impact testing equipment, (b) anti-rebounding device (c) fixture for holding a cylindrical specimen with mountings, and (d) post-impact filament wound cylindrical specimen.

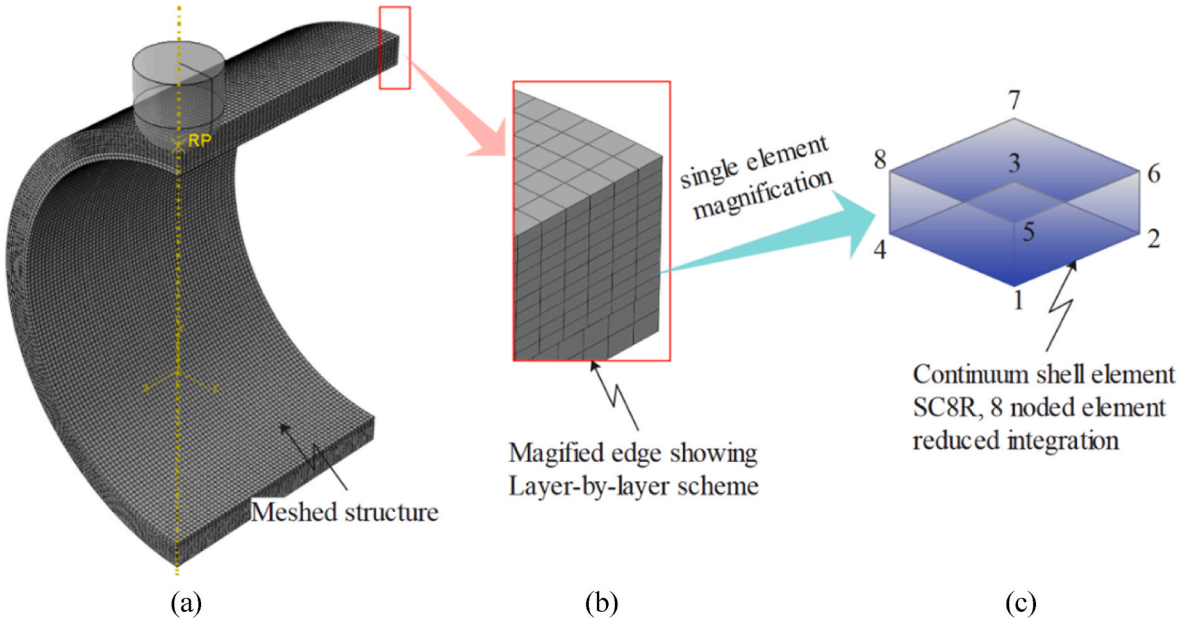

Fig. 4. (a) Mesh and element scheme (b) the layer-by-layer strategy is visually demonstrated, and (c) the continuum shell element details.

RIGID BODY constraint, or a deformable instance with assigned properties. Most studies treat the impactor as a rigid body [81–83]. The rigid body element in Abaqus FE software is designed for modeling solid, non-deformable bodies, making it ideal for simulating impact problems. It accurately represents rigid bodies colliding with each other and deformable bodies, captures time-dependent behavior in dynamic analyses, and allows for interactions between objects during events when used in conjunction with contact elements. This versatile tool is particularly useful for impact problem modeling and analysis, especially when used as an impactor in simulations. The assembled sample and impactor are shown in Fig. 5 (b).

3.3. Boundary conditions

Symmetry is a crucial aspect of FEA for simplifying and optimizing the modeling process. By dividing a structure into identical parts, a fraction of the structure can be analyzed and predicted based on symmetry assumptions. The approach to modeling symmetry depends on the type and degree of symmetry present. Faster analyses can be achieved by reducing the size and complexity of the model. Depending on the degree of symmetry, only one-quarter, one-half, or one-third of the structure needs to be modeled, accurately representing the entire structure's behavior. Appropriate boundary conditions are applied to the partial

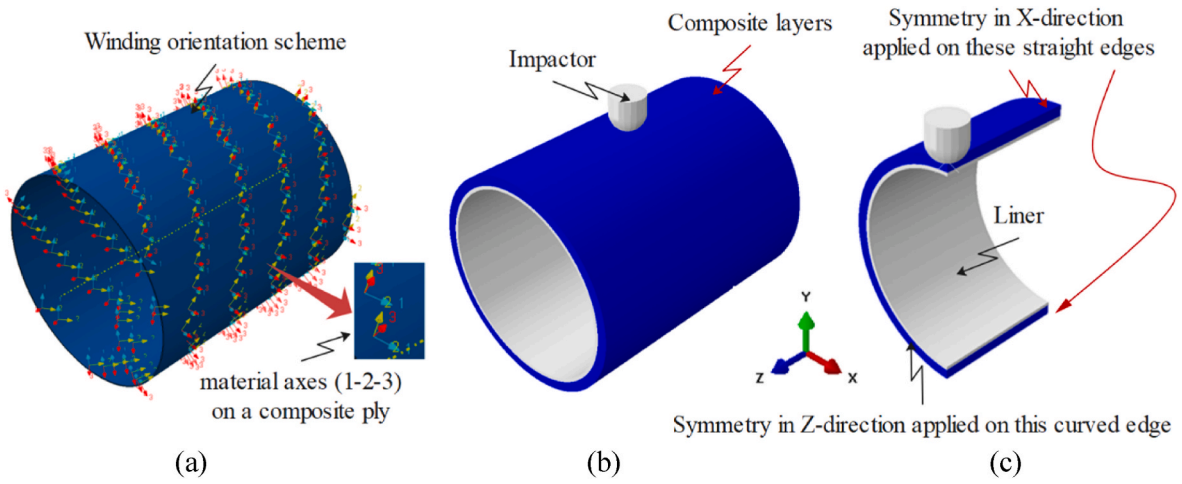

Fig. 5. Schematics of the cylindrical specimen: (a) winding orientation for a composite layer having 55° orientation during modeling (an example of a ply). The material axes are shown as a 1-2-3 orientation scheme, (b) a full view of the cylindrical sample, (c) a one-quarter view of the sample, showing the liner (white color) and the composite layers (blue color) and the edges on which symmetry is defined. (For interpretation of the references to color in this figure legend, the reader is referred to the Web version of this article).

model to ensure accurate results. Using symmetry in FEA offers substantial computational efficiency and reliable results for complex engineering problems. For the composite sample, symmetry was implemented at the straight and curved edges to align with the one-quarter approach. One-fourth depiction can be seen in Fig. 5 (c).

The impactor was designed to translate vertically downwards and strike the sample at the midpoint of its transverse plane. The space between the sample and the impactor is kept minimal to reduce step time. The initial condition for the impactor was defined as its velocity at the reference point, also a mass value was assigned to the rigid impactor at its reference point. The fixture, which securely holds the cylindrical specimen, is modeled as a rigid body. Fig. 6 provides an assembled view of the specimen, impactor, and V-block fixture.

3.4. Contact modeling

Contact modeling is a crucial step in FEA simulations, as it directly affects the accuracy of the results. Various methods define contact behavior; one is surface-to-surface contact, and the other is node-to-surface contact. The choice of master and slave surfaces depends on the deformation characteristics of the surfaces and the loading conditions. In general, the surface with smaller deformations is chosen as the

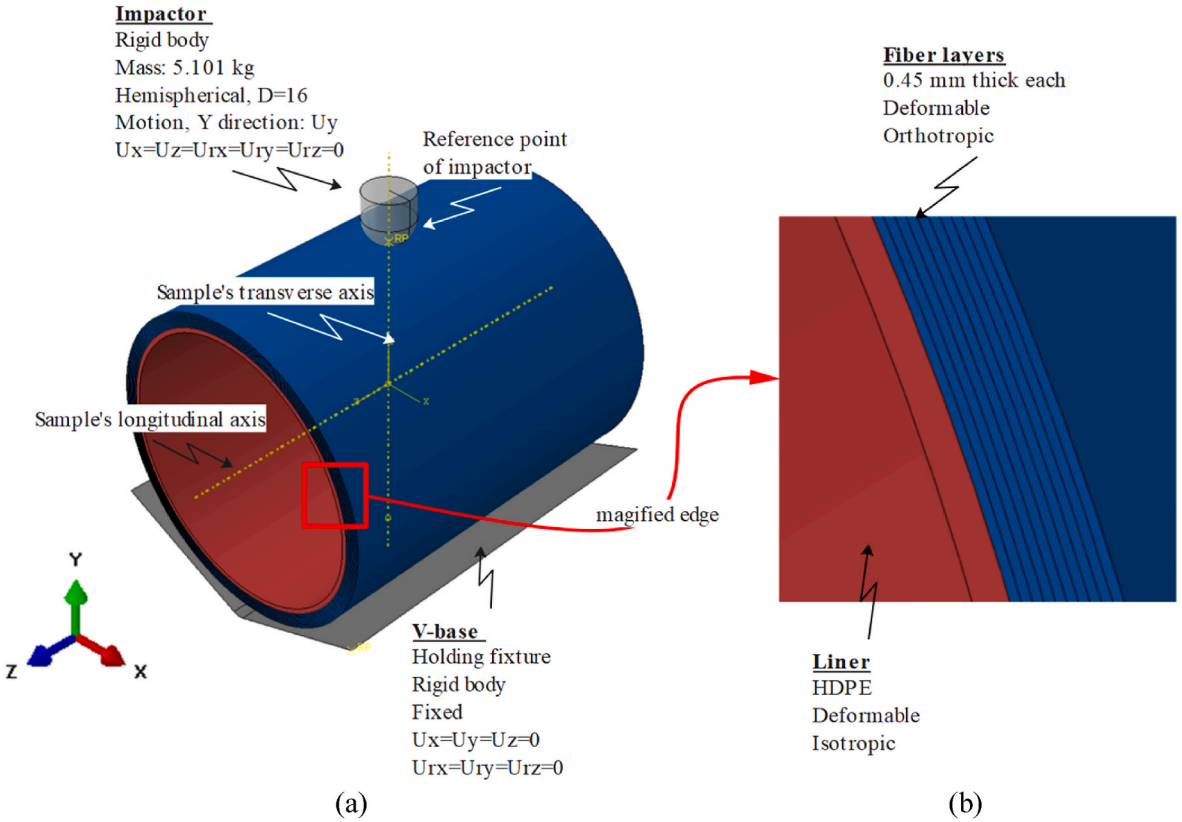

Fig. 6. Geometrical details of the composite sample, impactor, and V block: (a) assembled view showing the impactor hitting along the transverse axis of the sample. The V-base is held rigidly by constraining all the motions (b) the magnified edge of the sample showing the liner and the composite layers.

master to reduce computational costs and improve convergence. However, this is not always the situation, and one must carefully analyze the specific characteristics of the surfaces. When using a hard contact law, it is essential to define the contact surfaces accurately and specify the appropriate contact parameters [84]. This ensures that the simulation captures the contact surface behavior and produces reliable results. This study used the generic contact algorithm to simulate a low-velocity impact event between a rigid impactor and a target sample. The top ply's surface was designated as the slave surface, while the surface of the impactor was chosen as the master surface. A V-block support fixture was also created to represent the actual test fixture and connected to the composite specimen using a tie constraint. The geometrical details and assembly of various instances are shown in Fig. 6.

Fiber Tensile Failure Criterion for $\sigma_{11} \geq 0$;

$$\left(\frac{\sigma_{11}}{X_T}\right)^2 + \frac{\sigma_{12}^2 + \sigma_{13}^2}{S_{12}^2} = \begin{cases} \geq 1 & \text{failure} \\ < 1 & \text{no failure} \end{cases} \tag{1}$$

Fiber Compressive Failure Criterion for $\sigma_{11} < 0$;

$$\left(\frac{\sigma_{11}}{X_C}\right)^2 = \begin{cases} \geq 1 & \text{failure} \\ < 1 & \text{no failure} \end{cases} \tag{2}$$

Matrix Tensile Failure Criterion for $\sigma_{22} + \sigma_{33} > 0$;

$$\frac{(\sigma_{22} + \sigma_{33})^2}{Y_T^2} + \frac{\sigma_{23}^2 - \sigma_{22}\sigma_{33}}{S_{23}^2} + \frac{\sigma_{12}^2 + \sigma_{13}^2}{S_{12}^2} = \begin{cases} \geq 1 & \text{failure} \\ < 1 & \text{no failure} \end{cases} \tag{3}$$

Matrix Compressive Failure for $\sigma_{22} + \sigma_{33} < 0$;

$$\left[\left(\frac{Y_C}{2S_{23}}\right)^2 - 1\right]\left(\frac{\sigma_{22} + \sigma_{33}}{Y_C}\right) + \frac{(\sigma_{22} + \sigma_{33})^2}{4S_{23}^2} + \frac{\sigma_{23}^2 - \sigma_{22}\sigma_{33}}{S_{23}^2} + \frac{\sigma_{12}^2 + \sigma_{13}^2}{S_{12}^2} = \begin{cases} \geq 1 & \text{failure} \\ < 1 & \text{no failure} \end{cases} \tag{4}$$

3.5. Failure criteria

Failure criteria are essential for predicting the behavior of composites, and the Hashin criterion is one such model frequently used for this purpose [85]. The Hashin failure criterion reflects the relative strengths and stiffness of the matrix and fiber materials, to predict the composite's failure behavior under diverse loading types. This model is beneficial for predicting damage initiation and propagation in composites. The discrete damage modes inflicted by the low-velocity impact on composites include fiber breakage, matrix cracking, fiber-matrix debonding, etc. [86]. Matrix cracking appears when the matrix material cracks and fiber-matrix debonding occurs when the fibers separate from the matrix material. These damage modes can significantly affect the strength and stiffness of composite materials. Due to their inherent anisotropic properties, damage mechanisms in composites are frequently different from those seen in metals. For instance, fracture mechanisms that lower the material's strength and stiffness primarily provide impact energy absorption. Before the ultimate failure, at least several of these mechanisms typically occurs. However, metals have the potential to absorb energy through plastic deformation.

3.5.1. Damage initiation and evolution

Damage initiation states the process by which defects or damage occur and is the first symptom of damage to the laminate, leading to reduced mechanical performance in composite materials. Damage can appear due to several factors, including manufacturing defects, impact, fatigue, and environmental degradation. As soon as the damage starts, it spreads faster and with increased force. This process, known as damage evolution, weakens the composite laminate and reduce the robustness of the structure. This process is usually characterized by a decrease in the stiffness and strength of the composite material, leading to eventual failure [87]. A stress-based failure criteria approach or damage mechanics concepts can be employed to model damage initiation and evolution in composite laminates under the low-velocity impact. The damage initiation in the composite can be based on Hashin's failure criteria, which considers four unique damage mechanisms: fiber tension, fiber compression, matrix tension, and matrix [88,89]. Therefore, failure initiation must be completed to implement the damage evolution model [62]. The four indices that are numerically assessed are shown in Eqs. (1)–(4) for the four damage modes [90].

where σ_{ij}; $(i,j = 1,2,3)$ denotes the stress elements, and the lamina's allowable tensile and compressive strengths are denoted by T and C (subscripts), respectively. X_T, Y_T, Z_T, and X_C, Y_C, Z_C are the allowable tensile and compressive strengths. S_{12}, S_{13}, and S_{23} show allowable strengths in shear in the respective directions [91]. As the elements of a structure soften due to damage, the load within the structure is redistributed to adjacent elements, which can significantly impact the structure's overall behavior. The level of damage in an element is represented by a damage variable, which can take on different values depending on the simulated damage type. When the damage in an element reaches a certain level, i.e. the element can no longer carry any load, the loads being carried by that element are redistributed to adjacent elements. In the case of total damage, the damage variable will be equal to 1 for all integration points within the element, indicating that the element can no longer carry any load. The stiffness reduction due to damage can be modeled by introducing a damage variable, which represents the element's damage level, and reducing the element's stiffness matrix accordingly. The damage variable can be defined using different damage models commonly used to predict the onset and progression of damage in composite materials. Internal damage variables [92] that account for various damage types are mathematically written in Eqs. (5)–(7).

$$d_f = \begin{cases} d_f^t \text{ if } & \widehat{\sigma}_{11} \geq 0 \\ d_f^c \text{ if } & \widehat{\sigma}_{11} < 0 \end{cases}; \text{ the current state of fiber damage,} \tag{5}$$

$$d_m = \begin{cases} d_m^t \text{ if } & \widehat{\sigma}_{22} \geq 0 \\ d_m^c \text{ if } & \widehat{\sigma}_{22} < 0 \end{cases}; \text{ the current state of matrix damage,} \tag{6}$$

$$d_s = 1 - \left(1 - d_f^t\right)\left(1 - d_f^c\right)\left(1 - d_m^t\right)\left(1 - d_m^c\right); \quad \text{current state of shear damage,} \tag{7}$$

$$\sigma = C_d \varepsilon \tag{8}$$

$$C_d = \frac{1}{D}\begin{bmatrix} (1-d_f)E_{11} & (1-d_f)(1-d_m)\nu_{21}E_{11} & 0 \\ (1-d_f)(1-d_m)\nu_{12}E_{22} & (1-d_m)E_{22} & 0 \\ 0 & 0 & (1-d_s)GD \end{bmatrix} \tag{9}$$

$$D = 1 - (1-d_f)(1-d_m)\nu_{12}\nu_{21} \tag{10}$$

The damage evolution is calculated using Eq. (8), correlating between stress and strain in a damaged material where σ represents the stress, ε represents the strain, and C_d denotes the elastic modulus that defines the elasticity matrix, which reflects the damage-dependent elastic modulus in Eq. (9). The elastic modulus is a measure of the material's stiffness, and it changes as the damage progresses. As the damage initiates, the elastic modulus is reduced, decreasing the material's stiffness. This is reflected in Eq. (8) by the multiplication of the elastic modulus by the strain, resulting in a reduction of the stress. Also, various symbols have their usual meaning as E_{11} = Young's modulus (fiber direction), E_{22} = Young's modulus (transverse to the fibers), G = shear modulus, ν_{12} and ν_{21} are Poisson's ratios. D is the overall damage variable (Eq. (10)).

4. Results and discussion

Even minor impact damage can decrease vessel stress levels / burst pressure, leading to internal damage propagating over time, potentially causing catastrophic failure under pressure. Impactors transmit kinetic energy to samples, causing deformation and energy absorption through damage modes. Composites may suffer fiber breakage, matrix cracking, and fiber-matrix debonding. Experimental data from impact testing provides crucial information for evaluating responses. The contact force was determined using a force sensor and plotted versus time, as shown in Fig. 7 (black curve). The force-time curve from a low-velocity impact test provides valuable information about a material's mechanical behavior under impact loading conditions. It typically has two phases: loading (the load increases rapidly as the impactor contacts the sample) and unloading (the load decreases as the impactor rebounds). The slope near the peak force indicates stiffness, while the area beneath the curve represents the total energy absorbed. The rebound of the impactor after the peak force indicates the material's ability to store and release some absorbed energy, indicating its resilience.

The force-time curves obtained in the experimental study have an inverted bell-curve shape, indicating that the impactor did not perforated the specimen but rebounded, as depicted in Fig. 7 (a). The initial increase in load during low-velocity impact is due to the specimens' elastic response, followed by a decrease due to initial damage. As the impact continues, matrix cracks and propagates, leading to a gradual decrease in contact force. The maximum impact force (F_{peak}) represents the highest load recorded by the load cell, marking the end of the loading phase. The incident or damage threshold load (F_{init}) is the load at which material degradation begins, followed by amplitude fluctuations due to the evolution of failure modes on the sample. All samples remained unperforated against the 40 J energy level.

Additionally, Fig. 7 (b) displays matrix compression damage through FEA, illustrating the contact between the composite sample and the impactor during the impact event. The FEA shows deflection, rebounding, and a deformed face, with some impactor energy transmitting into the composite. Some of the impactor energy is transmitted into the composite, inducing damage, and the sample deflects back with the rebounding impactor due to the residual stiffness that remained in the sample.

The energy absorbed by a composite can be determined using an energy-time response plot, as shown in Fig. 7 (a) (blue dashed curve). This plot shows the relationship between the amount of impact energy absorbed by the sample and the duration of the impact event. It is used to evaluate the energy absorption and dissipation characteristics of the material. The peak in energy absorption occurs at the onset of impact, followed by a gradual decrease as the event progresses. A portion of the total impact energy is lost due to friction and vibration, while the rest is recovered by the impactor as residual elastic energy. The friction is more

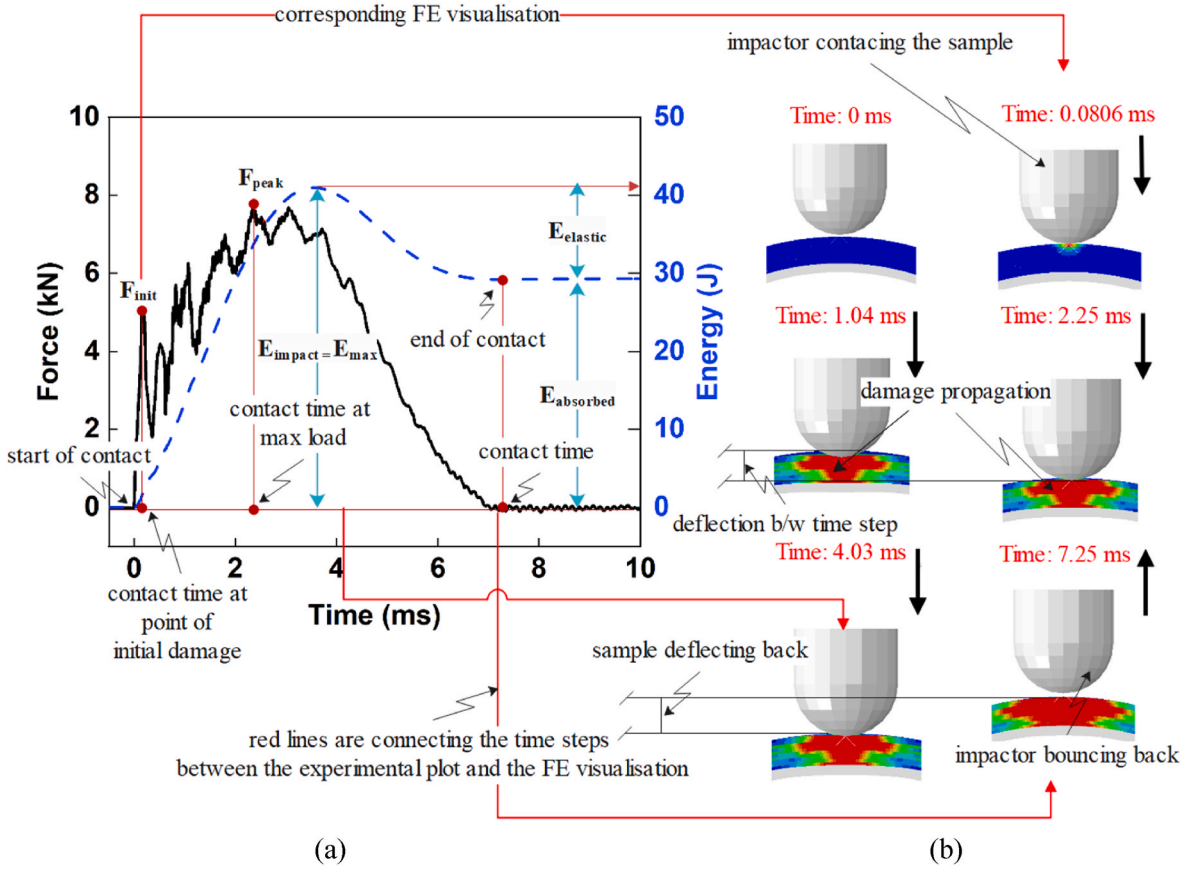

Fig. 7. (a) Force-time and energy-time response with various impact event features (b) Matrix compression damage is captured in various time steps, with the damage propagation and impactor rebound depicted.

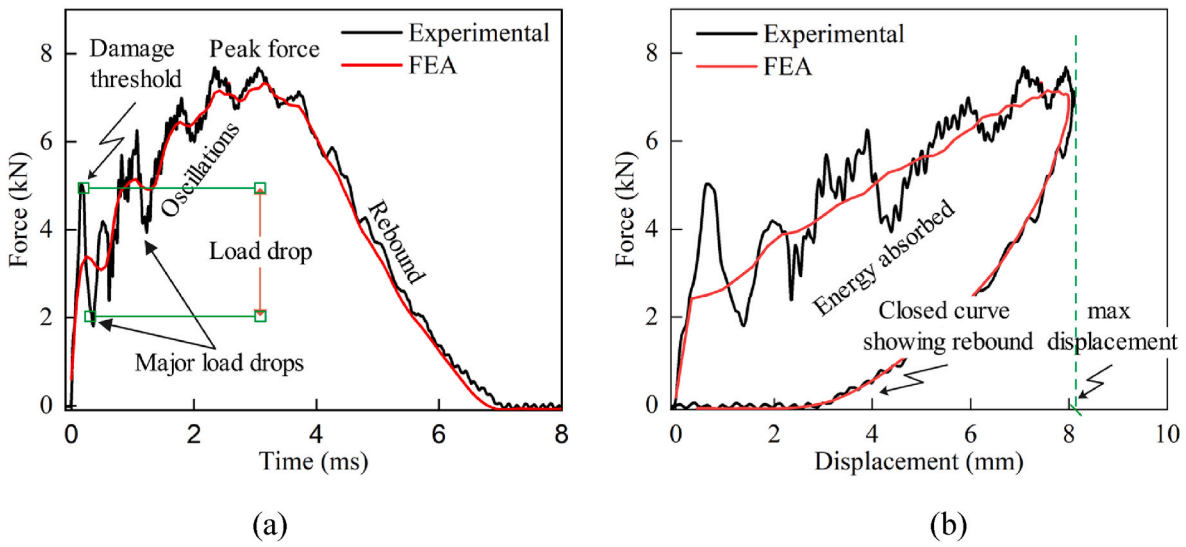

Fig. 8. Experiment and numerical plot comparison for (a) force-time and (b) force-displacement curves. However, the plots deviate little from each other at various stages for multiple reasons.

when penetration took place. The impactor rises because the rebound uses the remaining kinetic energy, also known as rebound/residual energy. When evaluating composite impact damage, it is common to discuss both impact energy (E_{impact} *or* E_{max}) and absorbed energy (E_{abs}). The absorbed energy reflects the energy lost by the system due to various mechanisms after the impactor makes contact with the target, including elastic deformation, friction, plastic deformation, and material damage [93]. The force-displacement curve measures the force applied to a composite sample, indicating the material's work and energy absorption capacity, Fig. 8 (b). It is crucial in determining the composite's damage resistance and energy absorption capacity. The maximum displacement gauge the component's ductility and energy absorption capacity. The force-displacement plot can provide insight into the composite's behavior during an impact event, allowing for recovery or permanent deformation. The force-time and force-displacement plots for experimental and FE studies show significant agreement, but slight disparities may be observed due to fabrication errors, voids, and defects, Fig. 8 (a) and (b).

Oscillations in the F-d curve during impact testing on composite materials are caused by the complex behavior of the material during the event. The composite material is comprised of multiple layers with variable features, which interact in a complex manner during the impact event. Damage onset results in fluctuations in load, leading to oscillations in the F-d curve. The dynamic nature of the event also causes oscillations, as the impactor impacts the material, causing it to deform, cause damage, and generate a force in the opposite direction. The amplitude and frequency of these fluctuations offer valuable insights into the behavior of material under impact loading. Deviations in

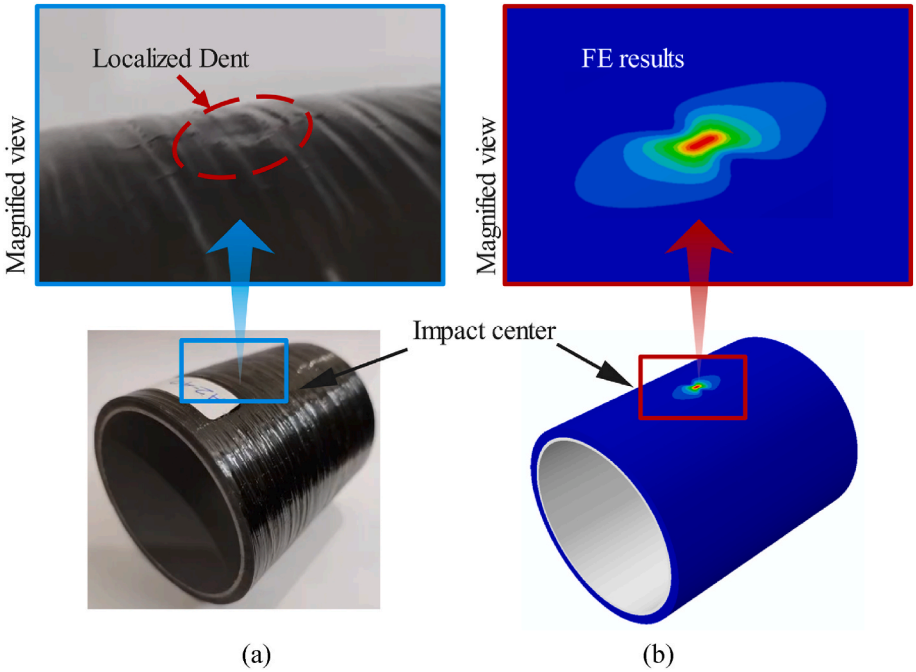

Fig. 9. Experimental and numerical captures on the surface of the sample, (a) experimental observation showing the localized dent, (b) FEA capture showing the Hashin fiber compression damage at the impact site.

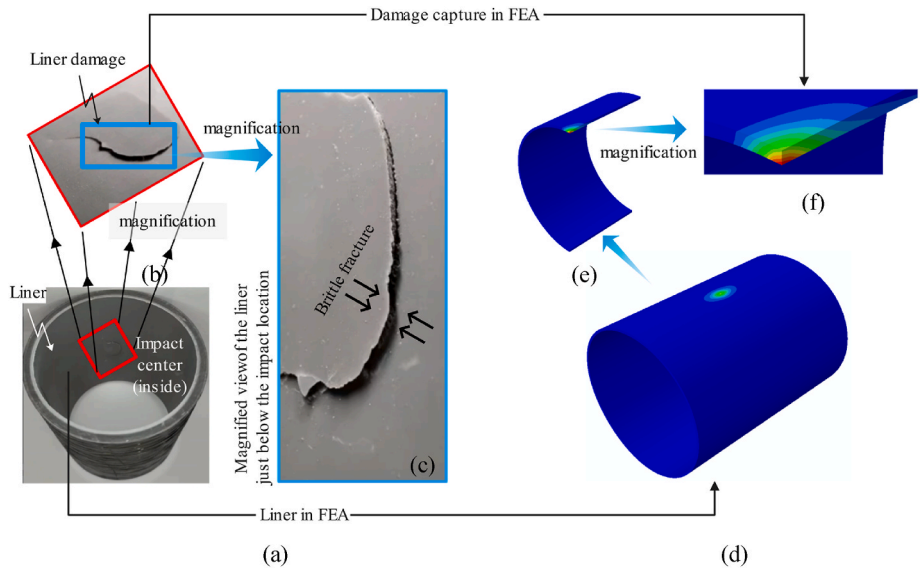

Fig. 10. Liner damage can be seen (a) from inside the sample, (b) from a close view of the damaged liner (c) from an enlarged view of the failure surface generated in the liner. The brittle fracture is shown in the enlarged view. (d) FE representation of liner. (e) Enlarged ¼ part with exposed edges (f) enlarged view of the exposed edge.

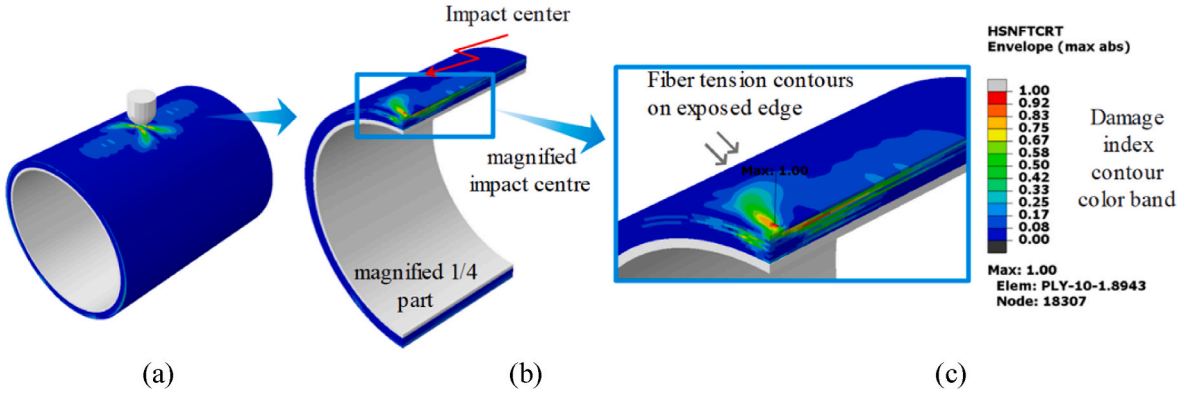

Fig. 11. Fiber tension damage is shown in the sample and the enlarged impact center and exposed edges: (a) full sample, (b) and (c) magnified impact center and edges showing fiber tension in the composite layers. The damage index contour band shows that the composite layers' fiber tension damage occurred (deep red areas). (For interpretation of the references to color in this figure legend, the reader is referred to the Web version of this article.)

experimental and FE curves can be caused by differences in material properties used in experiments and simulations, voids and fabrication errors, modeling assumptions and discretizing the numerical model.

Composite structures may experience matrix tensile cracking, matrix compressive failure, and fiber breakage due to transverse impact. Hashin's damage initiation criteria predict four damage types: fiber tension, fiber compression, matrix tension, and matrix compression [94]. The failure is anticipated based on the failure index or determination value (F) given (i.e., when F = 1) for each mode of damage criterion. Fig. 9 (a) shows the fiber compression effect on the cylindrical specimen, and the corresponding effect can be seen in the FE result in Fig. 9 (b).

Experimental and numerical findings capture localized compression at the impact site, which can conceal subsurface damages. Low-velocity impact indentation behavior in composite materials is influenced by factors like material qualities, impact conditions, etc. The impact on the surface can affect the liner and the bottom layer of structure and may cause damage in high-strain rate loadings. HDPE can exhibit brittle fracture at high strain rates, such as under-impact loads. The brittle fracture occurs when the material fails at a higher strain than it would under static loading [95]. This is due to the material not having enough time to deform plastically before it is subjected to a large amount of strain. As a result, the material is unable to dissipate the energy of the impact quickly enough, resulting in the material fracturing instead of deforming. A lack of plastic deformation characterizes this type of fracture, and the material breaks as brittle. As the strain rate increases, the material reach its brittle fracture point faster. Impact loads can cause the material to reach its brittle fracture point in a fraction of a second, leading to failure. Fig. 10 depicts the interior of the sample, where the sample's interior liner damage is clearly visible.

Fiber tension and compression damage in composite material at low-velocity impacts can occur due to the concentration of impact energy at the point of impact. When an impactor hits a composite material, the structure communicates the energy, causing fibers to stretch or compress. The brittle fibers are unable to absorb the impact energy, they may break or crack, resulting in fiber damage. Fiber tension damage is more likely to appear along the fiber orientation, as the fibers are subjected to the greatest amount of stretching in the direction parallel to the fibers, Fig. 11. Fiber compression damage is more likely in a composite material just at the point of impact.

5. Conclusions

Damage mechanisms in composite materials are often distinct from those observed in metals due to their unique anisotropic characteristics. The study investigates the dynamic behavior of carbon-fiber-wrapped structures during low-velocity impact events, focusing on the intricate interplay of forces and damage formations. It also explores the effect on the polymeric liners in the composite overwrapped structures. Production of CPVs and transmission pipes frequently uses the filament winding technique, where HDPE is extensively used as a liner material for diverse benefits. This study used the wet filament winding method to wound unidirectional carbon fibers with epoxy resin on a polymeric (HDPE) liner. BVID can lead to a decrease in the performance of composites and can be characterized in the form of damage forms that are barely visible to the naked eye. Experimental testing was performed on cylindrical specimens to understand the behavior of carbon/epoxy samples against low-velocity impact. An energy level of 40 J was adopted to establish the damage response of the specimen against impact. The impact damage states were characterized by surface damage, subsurface, and liner damage. Even though HDPE is a strong and flexible material, it can nevertheless break when subjected to high strain rates, such as those caused by impact loads. Brittle fractures in plastic liners can occur when they are subjected to impact loads. This failure mechanism is characterized by an abrupt, catastrophic break without considerable plastic deformation. Damage patterns were evident on both impacted and unimpacted sides, examined from the external damage observation. In FEA, the cylindrical specimen and impactor are modeled to mimic the experimental transverse impact test environment, representing the consequences of low-velocity impact. The computational model reproduces the impact response of the specimen, and various Hashin damage failure modes were captured through the simulation results. The impact damage seems to spread from the impact center with time. Minor fiber failures are predicted in the specimen. However, severe matrix damage took place at and around the impact locations.

Funding

This study was funded by the Ministry of Higher Education (MOHE), Malaysia, under the Fundamental Research Grant Scheme, grant number FRGS/1/2019/TK08/UTP/02/1.

CRediT authorship contribution statement

Mohammad Azeem: Conceptualization, Formal analysis, Investigation, Writing - original draft, Writing - review & editing. **Hamdan H. Ya:** Funding acquisition, Investigation. **Mohammad Azad Alam:** Data curation. **Masdi Muhammad:** Methodology, Resources, Supervision. **Salit M Sapuan:** Formal analysis, Visualization. **Mukesh Kumar:** Software. **Lokman Gemi:** Validation. **Ammar Maziz:** Resources. **Ahmad Rasdan Ismail:** Project administration, Resources. **Sanan H. Khan:** Data curation, Project administration, Writing - review & editing.

Declaration of competing interest

The authors declare that they have no known competing financial interests or personal relationships that could have appeared to influence the work reported in this paper.

Data availability

Data will be made available on request.

Acknowledgments

The authors would like to acknowledge and thank the Ministry of Higher Education (MOHE), Malaysia, and Universiti Teknologi PETRONAS for supporting this study. We are also thankful to SIRIM SDN. BHD. Penang, Malaysia, for supporting the fabrication process. We also extend our gratitude to Prof. Thariq H Sultan and Universiti Putra Malaysia for offering the experimental facility for this study.

References

[1] M. Reza Khoshravan Azar, A.A. Emami Satellou, M. Shishesaz, B. Salavati, Calculating the optimum angle of filament-wound pipes in natural gas transmission pipelines using approximation methods, J. Pressure Vessel Technol. 135 (2013) 1–7, https://doi.org/10.1115/1.4007189.

[2] A. Air, M. Shamsuddoha, B. Gangadhara Prusty, A review of Type V composite pressure vessels and automated fibre placement based manufacturing, Compos. Part B Eng. 253 (2023) 110573, https://doi.org/10.1016/j.compositesb.2023.110573.

[3] D.K. Rajak, D.D. Pagar, P.L. Menezes, E. Linul, Fiber-reinforced polymer composites: manufacturing, properties, and applications, Polymers 11 (2019), https://doi.org/10.3390/polym11101667.

[4] M. Azeem, H.H. Ya, M.A. Alam, M. Kumar, P. Stabla, M. Smolnicki, L. Gemi, R. Khan, T. Ahmed, Q. Ma, M.R. Sadique, A.A. Mokhtar, M. Mustapha, Application of filament winding technology in composite pressure vessels and challenges: a review, J. Energy Storage 49 (2022) 103468, https://doi.org/10.1016/j.est.2021.103468.

[5] B. Kim, B. Kim, J. Kim, C. Joe, Study on the development of composite CNG pressure vessels, Cryogenics 38 (1998) 131–134, https://doi.org/10.1016/S0011-2275(97)00123-9.

[6] C. Hopmann, N. Magura, R. Müller, D. Schneider, K. Fischer, Impact of winding parameters on the fiber bandwidth in the cylindrical area of a hydrogen pressure vessel for generating a digital twin, Polym. Compos. 43 (2022) 1577–1589, https://doi.org/10.1002/pc.26479.

[7] E. Lainé, J.C. Dupré, J.C. Grandidier, M. Cruz, Instrumented tests on composite pressure vessels (type IV) under internal water pressure, Int. J. Hydrogen Energy 46 (2021) 1334–1346, https://doi.org/10.1016/j.ijhydene.2020.09.160.

[8] S. Alam, G.R. Yandek, R.C. Lee, J.M. Mabry, Design and development of a filament wound composite overwrapped pressure vessel, Compos. Part C Open Access 2 (2020) 100045, https://doi.org/10.1016/j.jcomc.2020.100045.

[9] M. Azeem, H. Haji Ya, M. Azad Alam, M.R. Sadique, M.B. Mustapha, A. Akmar Bin Mokhtar, T. Ahmed, M.T.H. Sultan, R. Khan, Growth of NGVs and comparative study of cylinder material for CNG storage, in: Lect. Notes Mech. Eng., Springer Singapore, 2023, pp. 689–704, https://doi.org/10.1007/978-981-19-1939-8_54.

[10] C. Zhou, Z. Xia, Q. Yong, in: Micro Mechanical Model of Filament Wound Composite Pipe with Damage Analysis, vol. 3, 2006, pp. 67–74, https://doi.org/10.1115/PVP2006-ICPVT-11-93298. Des. Anal., ASMEDC.

[11] Y. Di Boon, S.C. Joshi, S.K. Bhudolia, Review: filament winding and automated fiber placement with in situ consolidation for fiber reinforced thermoplastic polymer composites, Polymers 13 (2021) 1951, https://doi.org/10.3390/polym13121951.

[12] S. Morkavuk, K. Aslantaş, L. Gemi, U. Köklü, Ş. Yazman, The influence of drilling-induced damages and hole quality on hoop tensile and fatigue behavior of CFRP tubes, Composites Part A: Applied Science and Manufacturing (2024) 108005, https://doi.org/10.1016/j.compositesa.2024.108005. In Press.

[13] D.S. Gemi, Ö.S. Şahin, L. Gemi, Experimental investigation of the effect of diameter upon low velocity impact response of glass fiber reinforced composite pipes, Compos. Struct. 275 (2021) 114428, https://doi.org/10.1016/j.compstruct.2021.114428.

[14] M.A. Karim, M.Z. Abdullah, A.F. Deifalla, M. Azab, A. Waqar, An assessment of the processing parameters and application of fibre-reinforced polymers (FRPs) in the petroleum and natural gas industries: a review, Res. Eng. 18 (2023) 101091, https://doi.org/10.1016/j.rineng.2023.101091.

[15] Z. Cui, Q. Liu, Y. Sun, Q. Li, On crushing responses of filament winding CFRP/aluminum and GFRP/CFRP/aluminum hybrid structures, Compos. Part B Eng. 200 (2020) 108341, https://doi.org/10.1016/j.compositesb.2020.108341.

[16] J.H.S. Almeida, M.L. Ribeiro, V. Tita, S.C. Amico, Damage and failure in carbon/epoxy filament wound composite tubes under external pressure: experimental and numerical approaches, Mater. Des. 96 (2016) 431–438, https://doi.org/10.1016/j.matdes.2016.02.054.

[17] N.H. Farhood, S. Karuppanan, H.H. Ya, M. Ovinis, Effects of carbon fiber hybridization on the compressive strength of glass-carbon/epoxy hybrid composite pipes before and after low velocity impact, Key Eng. Mater. 796 (2019) 30–37. https://doi.org/10.4028/www.scientific.net/KEM.796.30.

[18] H. Xia, C. Shi, J. Wang, X. Bao, H. Li, G. Fu, Effects of thickness and winding angle of reinforcement laminates on burst pressure capacity of thermoplastic composite pipes, J. Offshore Mech. Arctic Eng. 143 (2021) 1–8, https://doi.org/10.1115/1.4050060.

[19] G. Sun, Z. Wang, J. Hong, K. Song, Q. Li, Experimental investigation of the quasi-static axial crushing behavior of filament-wound CFRP and aluminum/CFRP hybrid tubes, Compos. Struct. 194 (2018) 208–225, https://doi.org/10.1016/j.compstruct.2018.02.005.

[20] N. Razali, M.T.H. Sultan, M. Jawaid, Impact Damage Analysis of Hybrid Composite Materials, Elsevier Ltd, 2018, https://doi.org/10.1016/B978-0-08-102290-0.00006-4.

[21] M.T.H. Sultan, A.U.M. Shah, N. Saba (Eds.), *Impact Studies of Composite Materials*, Springer, Singapore, 2021, https://doi.org/10.1007/978-981-16-1323-4.

[22] H. Tuo, Z. Lu, X. Ma, J. Xing, C. Zhang, Damage and failure mechanism of thin composite laminates under low-velocity impact and compression-after-impact loading conditions, Compos. Part B Eng. 163 (2019) 642–654, https://doi.org/10.1016/j.compositesb.2019.01.006.
[23] H. Cui, D. Thomson, S. Eskandari, N. Petrinic, A critical study on impact damage simulation of IM7/8552 composite laminate plate, Int. J. Impact Eng. 127 (2019) 100–109, https://doi.org/10.1016/j.ijimpeng.2019.01.009.
[24] I. Papa, A. Formisano, V. Lopresto, A. Langella, Low velocity impact behaviour of reinforced plastic laminates: indentation and penetration laws validated for different fibres and matrices, Compos. Part B Eng. 164 (2019) 61–66, https://doi.org/10.1016/j.compositesb.2018.11.070.
[25] W. Ao, W. Zhuang, B. Xing, Q. Zhou, Y. Xia, Finite element method of a progressive intralaminar and interlaminar damage model for woven fibre laminated composites under low velocity impact, Mater. Des. 223 (2022) 111256, https://doi.org/10.1016/j.matdes.2022.111256.
[26] S.K. Bhudolia, G. Gohel, J. Kantipudi, K.F. Leong, P. Gerard, Manufacturing and investigating the load, energy and failure attributes of thin ply carbon/Elium® thermoplastic hollow composites under low-velocity impact, Mater. Des. 206 (2021), https://doi.org/10.1016/j.matdes.2021.109814.
[27] L. Ferrante, F. Sarasini, J. Tirillò, L. Lampani, T. Valente, P. Gaudenzi, Low velocity impact response of basalt-aluminium fibre metal laminates, Mater. Des. 98 (2016) 98–107, https://doi.org/10.1016/j.matdes.2016.03.002.
[28] L. Gemi, Investigation of the effect of stacking sequence on low velocity impact response and damage formation in hybrid composite pipes under internal pressure. A comparative study, Composites Part B: Eng 153 (2018) 217–232. https://doi.org/10.1016/j.compositesb.2018.07.056.
[29] N.H. Farhood, S. Karuppanan, H.H. Ya, M. Ovinis, Experimental study of low velocity impact response of carbon/basalt hybrid filament wound composite pipes, Int. J. Struct. Stabil. Dynam. 18 (2018) 1850089, https://doi.org/10.1142/S021945541850089X.
[30] M.L. Ribeiro, D. Vandepitte, V. Tita, Experimental analysis of transverse impact loading on composite cylinders, Compos. Struct. 133 (2015) 547–563, https://doi.org/10.1016/j.compstruct.2015.07.088.
[31] L. Gemi, M. Kayrıcı, M. Uludağ, D.S. Gemi, Ö.S. Şahin, Experimental and statistical analysis of low velocity impact response of filament wound composite pipes, Compos. Part B Eng. 149 (2018) 38–48, https://doi.org/10.1016/j.compositesb.2018.05.006.
[32] L. Gemi, Ö. S Şahin, A. Akdemir, Experimental investigation of fatigue damage formation of hybrid pipes subjected to impact loading under internal pre-stress, Compos. Part B Eng. 119 (2017) 196–205, https://doi.org/10.1016/j.compositesb.2017.03.051.
[33] J.H.S. Almeida, M.L. Ribeiro, V. Tita, S.C. Amico, Damage modeling for carbon fiber/epoxy filament wound composite tubes under radial compression, Compos. Struct. 160 (2017) 204–210, https://doi.org/10.1016/j.compstruct.2016.10.036.
[34] E.S. Barboza Neto, M. Chludzinski, P.B. Roese, J.S.O. Fonseca, S.C. Amico, C. A. Ferreira, Experimental and numerical analysis of a LLDPE/HDPE liner for a composite pressure vessel, Polym. Test. 30 (2011) 693–700, https://doi.org/10.1016/j.polymertesting.2011.04.016.
[35] D.S. Gemi, Ö.S. Şahin, L. Gemi, Experimental investigation of axial compression behavior after low velocity impact of glass fiber reinforced filament wound pipes with different diameter, Compos. Struct. 280 (2022), https://doi.org/10.1016/j.compstruct.2021.114929.
[36] L. Ma, F. Liu, D. Liu, Y. Liu, Review of strain rate effects of fiber-reinforced polymer composites, Polymers 13 (2021), https://doi.org/10.3390/polym13172839.
[37] British Standard EN 14767, LPG Equipment and Accessories Transportable Refillable Composite Cylinders for Liquefied Petroleum Gas (LPG) Periodic Inspection, 2005.
[38] S. Kobayashi, M. Kawahara, Effects of stacking thickness on the damage behavior in CFRP composite cylinders subjected to out-of-plane loading, Compos. Part A Appl. Sci. Manuf. 43 (2012) 231–237, https://doi.org/10.1016/j.compositesa.2011.10.004.
[39] H.U. Khalid, M.C. Ismail, N. Nosbi, Permeation damage of polymer liner in oil and gas pipelines: a review, Polymers 12 (2020) 1–31, https://doi.org/10.3390/polym12102307.
[40] N.S. Zakaria, Z.M.A. Merican, M.F. Hamza, Performance and critical issues of polymer liners in pipeline industry : a review, Mater. Today Proc. 16 (2019) 2389–2397, https://doi.org/10.1016/j.matpr.2019.06.143.
[41] M. Legault, Pressure Vessel Tank Types | CompositesWorld, CompositesWorld, 2012. https://www.compositesworld.com/articles/pressure-vessel-tank-types. (Accessed 20 October 2021).
[42] W. Zhou, J. Wang, Z. Pan, J. Liu, L. Ma, J. Zhou, Y. Su, Review on optimization design, failure analysis and non-destructive testing of composite hydrogen storage vessel, Int. J. Hydrogen Energy (2022), https://doi.org/10.1016/j.ijhydene.2022.09.028.
[43] H. Barthelemy, M. Weber, F. Barbier, Hydrogen storage: recent improvements and industrial perspectives, Int. J. Hydrogen Energy 42 (2017) 7254–7262, https://doi.org/10.1016/j.ijhydene.2016.03.178.
[44] C.T. Bellehumeur, J.S. Tiang, Simulation of non-isothermal melt densification of polyethylene in rotational molding, Polym. Eng. Sci. 42 (2002) 215–229, https://doi.org/10.1002/pen.10942.
[45] Y. Su, H. Lv, W. Zhou, C. Zhang, Review of the hydrogen permeability of the liner material of type iv on-board hydrogen storage tank, World Electr. Veh. J. 12 (2021) 1–18, https://doi.org/10.3390/wevj12030130.
[46] B. Gentilleau, F. Touchard, J.C. Grandidier, Numerical study of influence of temperature and matrix cracking on type IV hydrogen high pressure storage vessel behavior, Compos. Struct. 111 (2014) 98–110, https://doi.org/10.1016/j.compstruct.2013.12.034.
[47] X. Wang, M. Tian, X. Chen, P. Xie, J. Yang, J. Chen, W. Yang, Advances on materials design and manufacture technology of plastic liner of type IV hydrogen storage vessel, Int. J. Hydrogen Energy 47 (2022) 8382–8408, https://doi.org/10.1016/j.ijhydene.2021.12.198.
[48] M.R. Usman, Hydrogen storage methods: review and current status, Renew. Sustain. Energy Rev. 167 (2022) 112743, https://doi.org/10.1016/j.rser.2022.112743.
[49] M.S. Laad, Polymers in Sports, INC, 2020, https://doi.org/10.1016/B978-0-12-816808-0.00015-9.
[50] M. Amjadi, A. Fatemi, Tensile behavior of high-density polyethylene including the effects of processing technique, thickness, temperature, and strain rate, Polymers 12 (2020), https://doi.org/10.3390/POLYM12091857.
[51] N.H. Farhood, Low velocity impact simulation of cylindrical section for type IV composite pressure vessels, AIP Conf. Proc. (2021) 150001, https://doi.org/10.1063/5.0065443.
[52] S. Sapre, K. Pareek, M. Vyas, Investigation of structural stability of type IV compressed hydrogen storage tank during refueling of fuel cell vehicle, Energy Storage 2 (2020) 1–11, https://doi.org/10.1002/est2.150.
[53] N.H. Farhood, S. Karuppanan, H.H. Ya, M.T.H. Sultan, Experimental investigation on the effects of glass fiber hybridization on the low-velocity impact response of filament-wound carbon-based composite pipes, Polym. Polym. Compos. 29 (2021) 829–841, https://doi.org/10.1177/0967391120938181.
[54] J.C. Velosa, J.P. Nunes, P.J. Antunes, J.F. Silva, A.T. Marques, Development of a new generation of filament wound composite pressure cylinders, Compos. Sci. Technol. 69 (2009) 1348–1353, https://doi.org/10.1016/j.compscitech.2008.09.018.
[55] A. Hocine, A. Ghouaoula, F.K. Achira, S.M. Medjdoub, F. Kara Achira, S. M. Medjdoub, Analysis of failure pressures of composite cylinders with a polymer liner of type IV CNG vessels, Int. J. Mech. Ind. Sci. Eng. 7 (2013) 148–152, https://doi.org/10.5281/zenodo.1327839.
[56] G.B. Chai, P. Manikandan, Low velocity impact response of fibre-metal laminates - a review, Compos. Struct. 107 (2014) 363–381, https://doi.org/10.1016/j.compstruct.2013.08.003.
[57] E. Ozaslan, A. Yetgin, B. Acar, V. Coskun, T. Olgar, The effects of layer-by-layer thickness and fiber volume fraction variation on the mechanical performance of a pressure vessel, J. Press. Vessel Technol. Trans. ASME. 142 (2020) 1–6, https://doi.org/10.1115/1.4046655.
[58] H. Fang, D. Wang, Simulation analysis of delamination damage for the thick-walled composite-overwrapped pressure vessels, Materials 15 (2022), https://doi.org/10.3390/ma15196880.
[59] K.L. Alderson, K.E. Evans, Failure mechanisms during the transverse loading of filament-wound pipes under static and low velocity impact conditions, Composites 23 (1992) 167–173, https://doi.org/10.1016/0010-4361(92)90437-Y.
[60] G. Irven, A. Duncan, A. Whitehouse, D. Carolan, A. Fergusson, J.P. Dear, Impact response of composite sandwich structures with toughened matrices, Mater. Des. 203 (2021), https://doi.org/10.1016/j.matdes.2021.109629.
[61] E. Randjbaran, R. Zahari, N.A. Abdul Jalil, D.L. Abang Abdul Majid, Hybrid composite laminates reinforced with kevlar/carbon/glass woven fabrics for ballistic impact testing, Sci. World J. 2014 (2014) 1, https://doi.org/10.1155/2014/413753. –7.
[62] M. Azeem, H.H. Ya, M.A. Alam, T.H. Sultan, M. Ali, M. Sattar, T. Ahmad, H. Hatami, M.R. Sadique, A.A. Mokhtar, M. Mustapha, M.A. Khan, F. Masood, Macroscale assessment of low-velocity impact on hybrid composite laminates, Mater. Werkst. 52 (2021) 1101–1111, https://doi.org/10.1002/mawe.202000325.
[63] X.C. Sun, S.R. Hallett, Barely visible impact damage in scaled composite laminates: experiments and numerical simulations, Int. J. Impact Eng. 109 (2017) 178–195, https://doi.org/10.1016/j.ijimpeng.2017.06.008.
[64] W.J. Cantwell, J. Morton, The impact resistance of composite materials — a review, Composites 22 (1991) 347–362, https://doi.org/10.1016/0010-4361(91)90549-V.
[65] S. Abrate, Impact on laminated composites: recent advances, Appl. Mech. Rev. 47 (1994) 517–544, https://doi.org/10.1115/1.3111065.
[66] P.A. Arrabiyeh, D. May, M. Eckrich, A.M. Dlugaj, An overview on current manufacturing technologies: processing continuous rovings impregnated with thermoset resin, Polym. Compos. (2021) 26274, https://doi.org/10.1002/pc.26274.
[67] F.L. Jin, X. Li, S.J. Park, Synthesis and application of epoxy resins: a review, J. Ind. Eng. Chem. 29 (2015) 1–11, https://doi.org/10.1016/j.jiec.2015.03.026.
[68] M. Peerzada, S. Abbasi, K.T. Lau, N. Hameed, Additive manufacturing of epoxy resins: materials, methods, and latest trends, Ind. Eng. Chem. Res. 59 (2020) 6375–6390, https://doi.org/10.1021/acs.iecr.9b06870.
[69] V. Fiore, A. Valenza, Epoxy Resins as a Matrix Material in Advanced Fiber-Reinforced Polymer (FRP) Composites, 2013, https://doi.org/10.1533/9780857098641.1.88.
[70] F. Sarasini, Low-velocity Impact Behaviour of Hybrid Composites, Elsevier Ltd, 2017, https://doi.org/10.1016/B978-0-08-100787-7.00007-X.
[71] Q. Wang, T. Li, B. Wang, C. Liu, Q. Huang, M. Ren, Prediction of void growth and fiber volume fraction based on filament winding process mechanics, Compos. Struct. 246 (2020) 112432, https://doi.org/10.1016/j.compstruct.2020.112432.
[72] M. Azeem, H.H. Ya, M. Azad Alam, M. Kumar, Z. Sajid, S. Gohari, A. Maziz, L. Gemi, A. Syed, S.H. Khan, Influence of winding angles on hoop stress in composite pressure vessels: Finite element analysis, Res. Eng. 21 (2024), 101667–101667, https://doi.org/10.1016/j.rineng.2023.101667.

[73] S.Z.H. Shah, P.S.M. Megat-Yusoff, S. Karuppanan, R. Choudhry, Z. Sajid, Multiscale damage modelling of 3D woven composites under static and impact loads, Compos. Part A Appl. Sci. Manuf. 151 (2021) 106659, https://doi.org/10.1016/j.compositesa.2021.106659.
[74] M. Kaddeche, K. Chaoui, M.A. Yallese, Cutting parameters effects on the machining of two high density polyethylene pipes resins, Mec. Ind. 13 (2012) 307–316, https://doi.org/10.1051/meca/2012029.
[75] X. Li, D. Ma, H. Liu, W. Tan, X. Gong, C. Zhang, Y. Li, Assessment of failure criteria and damage evolution methods for composite laminates under low-velocity impact, Compos. Struct. 207 (2019) 727–739, https://doi.org/10.1016/j.compstruct.2018.09.093.
[76] R. Rafiee, M.A. Torabi, M.A.T. R Rafiee, Stochastic prediction of burst pressure in composite pressure vessels, Compos. Struct. 185 (2018) 573–583, https://doi.org/10.1016/j.compstruct.2017.11.068.
[77] K. Lasn, N.P. Vedvik, A.T. Echtermeyer, The sensitivity of the burst performance of impact damaged pressure vessels to material strength properties, IOP Conf. Ser. Mater. Sci. Eng. 139 (2016) 012029, https://doi.org/10.1088/1757-899X/139/1/012029.
[78] S.M.R. Khalili, M. Soroush, A. Davar, O. Rahmani, Finite element modeling of low-velocity impact on laminated composite plates and cylindrical shells, Compos. Struct. 93 (2011) 1363–1375, https://doi.org/10.1016/j.compstruct.2010.10.003.
[79] R. Rafiee, F. Abbasi, Numerical and experimental analyses of the hoop tensile strength of filament-wound composite tubes, Mech. Compos. Mater. 56 (2020) 423–436, https://doi.org/10.1007/s11029-020-09894-2.
[80] P.F. Liu, L.J. Xing, J.Y. Zheng, Failure analysis of carbon fiber/epoxy composite cylindrical laminates using explicit finite element method, Compos. Part B Eng. 56 (2014) 54–61, https://doi.org/10.1016/j.compositesb.2013.08.017.
[81] L.S. Kistler, A.M. Waas, On the response of curved laminated panels subjected to transverse impact loads, Int. J. Solid Struct. 36 (1999) 1311–1327, https://doi.org/10.1016/S0020-7683(98)00005-5.
[82] M. Tarfaoui, P.B. Gning, L. Hamitouche, Dynamic response and damage modeling of glass/epoxy tubular structures: numerical investigation, Compos. Part A Appl. Sci. Manuf. 39 (2008) 1–12, https://doi.org/10.1016/j.compositesa.2007.10.001.
[83] S.H. Khan, A.P. Sharma, R. Kitey, V. Parameswaran, Effect of metal layer placement on the damage and energy absorption mechanisms in aluminium/glass fibre laminates, Int. J. Impact Eng. 119 (2018) 14–25, https://doi.org/10.1016/j.ijimpeng.2018.04.011.
[84] Abaqus, Analysis User's Manual, vols. I-IV, 2010.
[85] A. Maziz, M. Tarfaoui, L. Gemi, S. Rechak, M. Nachtane, A progressive damage model for pressurized filament-wound hybrid composite pipe under low-velocity impact, Compos. Struc. 276 (2021), 114520–114520, https://doi.org/10.1016/j.compstruct.2021.114520.
[86] S. Nur Azrie Bt Safri, M.T.H. Sultan, M. Jawaid, Damage analysis of glass fiber reinforced composites, Durab. Life Predict. Biocomposites, Fibre-Reinforced Compos. Hybrid Compos. (2018) 133–147, https://doi.org/10.1016/B978-0-08-102290-0.00007-6.
[87] Y. Shi, T. Swait, C. Soutis, Modelling damage evolution in composite laminates subjected to low velocity impact, Compos. Struct. 94 (2012) 2902–2913, https://doi.org/10.1016/j.compstruct.2012.03.039.
[88] Y. Shi, C. Soutis, A finite element analysis of impact damage in composite laminates, Aeronaut. J. 116 (2012) 1331–1347, https://doi.org/10.1017/S0001924000007661.
[89] K.A. Kamarudin, M.K.M. Nor, A.E. Ismail, I.A. Hamid, A.S. Abdullah, Progressive damage modeling of synthetic fiber polymer composites under ballistic impact, Model. Damage Process. Biocompos. Fibre-Reinforced Compos. Hybrid Compos. (2018) 115–132, https://doi.org/10.1016/B978-0-08-102289-4.00007-2.
[90] Y. Abdel-Nasser, A.M.H. Elhewy, I. Al-Mallah, Impact analysis of composite laminate using finite element method, Ships Offshore Struct. 12 (2017) 219–226. https://doi.org/10.1080/17445302.2015.1131005.
[91] V. Gattineni, V. Nathi, Pre-stressed thin tubular composite energy absorbers for improved impact energy absorption, Res. Eng. 5 (2020) 100102, https://doi.org/10.1016/j.rineng.2020.100102.
[92] A. Maziz, M. Tarfaoui, S. Rechak, M. Nachtane, L. Gemi, Finite Element Analysis of Impact-Induced Damage in Pressurized Hybrid Composites Pipes, Intern. J. Appl. Mech. 13 (07) (2021) 2150074. https://doi.org/10.1142/s1758825121500745.
[93] F. Sarasini, J. Tirillò, L. Ferrante, M. Valente, T. Valente, L. Lampani, P. Gaudenzi, S. Cioffi, S. Iannace, L. Sorrentino, Drop-weight impact behaviour of woven hybrid basalt–carbon/epoxy composites, Compos. Part B Eng. 59 (2014) 204–220, https://doi.org/10.1016/j.compositesb.2013.12.006.
[94] R.F. Alshahrani, N. Merah, S.M.A. Khan, Y. Al-Nassar, On the impact-induced damage in glass fiber reinforced epoxy pipes, Int. J. Impact Eng. 97 (2016) 57–65, https://doi.org/10.1016/j.ijimpeng.2016.06.002.
[95] H. Pan, S. Devasahayam, S. Bandyopadhyay, Study of microstructure and fracture properties of blunt notched and sharp cracked high density polyethylene specimens, Sci. Rep. 7 (2017) 1–13, https://doi.org/10.1038/s41598-017-03884-6.